

Formation of Groups and Clusters of Galaxies

Alexander Knebe and Volker Müller

Astrophysikalisches Institut Potsdam, An der Sternwarte 16, D-14482 Potsdam, Germany

Received date; accepted date

Abstract. The formation, inner properties, and spatial distribution of galaxy groups and clusters are closely related to the background cosmological model. We use numerical simulations of variants of the CDM model with different cosmological parameters and distinguish relaxed objects from recent mergers using the degree of virialisation. Mergers occur mostly in deep potential wells and mark the most important structure formation processes. As consequence, the autocorrelation function of merged halos has a higher amplitude and is steeper than that of the virialized clusters. This can be directly connected to the same result found from the observation of luminous infrared galaxies; they are as well more strongly correlated and can primarily be identified with ongoing merging events.

Key words: cosmology - galaxy clusters - structure formation - numerical simulations

1. Introduction

Gravitational instability is commonly accepted as the basic mechanism for structure formation on large scales. Combined with the CDM model it leads to the picture of hierarchical clustering with wide support from deep galaxy and cluster observations. During the recent phase of cosmic evolution groups and clusters of galaxies condense from large scale density enhancements, and they grow by accretion and merger processes of the environmental cosmic matter. We expect traces of such recent formation processes still in presently observed objects, such as deviations from virial equilibrium, eccentric shapes, and substructures. X-ray observations of clusters show a large variety of morphologies which hopefully could discriminate between different cosmologies (Mohr et al. 1995). In low Ω_0 universes structure formation ceases at earlier times compared to cosmological models with a higher value for the density parameter. In the contrary, recent simulations show a remarkable similarity of internal structures as the average density profile when they are compared at rescaled radii normalized to a typical scale as the virial radius (Jing et al. 1995, Thomas et al. 1997). For these analysis they concentrate on a sample of isolated clusters in high resolution cosmological

simulations which emphasizes the relaxed structure found. In the contrary, we intend to concentrate on the appearance and the clustering of a sample of simulated clusters showing evidence of perturbations and interaction. We discuss cluster formation using dissipationless N -body simulations of variants of the CDM model with different cosmological parameters Ω_0 , Λ_0 , and $H_0 = 100h \text{ km s}^{-1}\text{Mpc}^{-1}$, where h is the Hubble parameter in units of $100 \text{ km s}^{-1}\text{Mpc}^{-1}$. Our goal is to interpret the simulated data of the structure and spatial distribution of groups and clusters which can discriminate between the models, and which can also help to get an understanding of the physics underlying the formation of these objects.

One of the critical questions in N -body simulations is the identification of groups and clusters of galaxies. There are several methods such as the standard friends-of-friends algorithm (FOF) introduced by Davis et al. (1985), the spherical overdensity method described by Lacey & Cole (1994) or more refined algorithm just as the DENMAX procedure (Gelb & Bertschinger 1994) or the hierarchical FOF group finding (Klypin et al. 1997). But it is by no means clear which of these methods best fits the observational procedures for identifying groups and clusters of galaxies. We decided to use the standard FOF group finder because this algorithm picks up particle groups without preferring any special geometry. Additionally we adopted the virial theorem: particle groups that do not obey this relation are investigated in detail. Visual inspection of such objects often shows the FOF group finder's tendency to link separate groups by small bridges, and groupings of particles with strongly discordant velocities. Quantifying their number and specifics helps in understanding some of the most impressive objects in the large scale matter distribution of the universe. We should remark that among the unvirialized groups, there exists a number of low mass badly resolved objects which are not of interest in this study.

The outline of the paper is as follows. First we specify the N -body simulations. Next we discuss the cluster halos and their properties. In Section 4 we study the spatial clustering of the different groups. We conclude with a discussion of our main results.

2. Cosmological N -body simulations

We base our analysis on four cosmological models all with an amplitude as measured by the 4-year COBE experiment, cf. Bunn & White (1997). First we take the standard CDM-model, with critical mass density $\Omega_0 = 1$ and a dimensionless Hubble constant $h = 0.5$, which is used as a reference in spite of the difficulty in reproducing both large and small scale clustering. More realistic variants of the CDM model have a lower matter content, as Λ CDM and OCDM1, which both have $\Omega_0 = 0.3$, and $h = 0.7$. For these models the shape parameter of the power spectrum $\Gamma \equiv \Omega_0 h = 0.21$ better fits the constraints from galaxy and cluster clustering, (e.g. Peacock & Dodds 1996, Einasto et al. 1998). The models were normalized to the full 4-year COBE signal using the Boltzmann code CMBFAST developed by Seljak & Zaldarriaga (1996) and assuming a baryon content of $\Omega_b h^2 = 0.0125$ suggested by big bang nucleosynthesis. The mass variance of the linear input spectrum at a scale of $8h^{-1}\text{Mpc}$ is given by σ_8 . Finally we used a less extreme open model OCDM2 with $\Omega_0 = 0.5$ which promises realistic large scale galaxy clustering and has the same mass variance at $8h^{-1}\text{Mpc}$ as galaxies. The information about the models can be found in Table 1.

Table 1. Physical properties of the numerical simulations. The box size L is given in $h^{-1}\text{Mpc}$, the particle mass m_p in units of $10^{11} h^{-1}\text{M}_\odot$.

	Ω_0	$\Omega_{\Lambda,0}$	h	σ_8	L	m_p
SCDM	1.0	0.0	0.5	1.18	200	11.0
ΛCDM	0.3	0.7	0.7	1.00	280	8.7
OCDM1	0.3	0.0	0.7	0.48	280	8.7
OCDM2	0.5	0.0	0.7	0.96	280	15.0

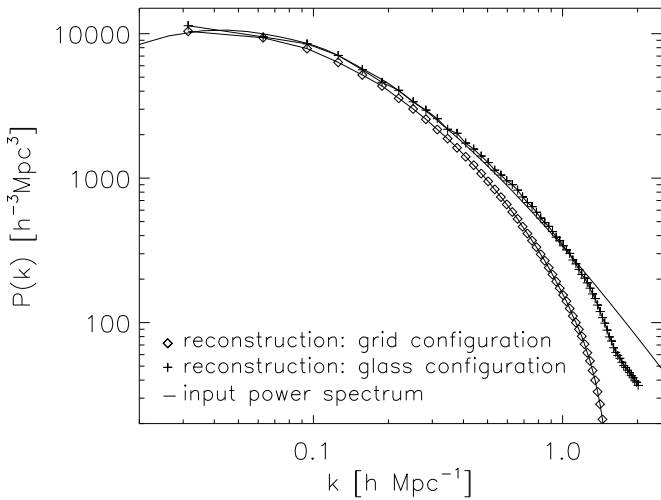


Fig. 1. Power spectrum reconstructed from the initial configuration (glass and grid starting points) for the SCDM model in comparison to the theoretical input spectrum.

We employ a ‘glass’ initial particle distribution (White 1996, cf. also Couchman et al. 1995) and use the Zeldovich approximation for initial displacements and initial velocities according to the specified power spectrum. In Fig. 1 we illustrate the improvement in the reproduction of the spectrum in using the irregular versus a grid initial particle distribution. The evolution of the gravitating system of dark matter particles is simulated with the adaptive P³M code (Couchman 1991), adapted to arbitrary background cosmological models. The simulations are started at redshift $z = 25$ and run with 128^3 particles on a 128^3 grid with a force resolution of $50 h^{-1}\text{kpc}$ (comoving).

3. Cluster Halos and their Properties

Groups and clusters of galaxies are identified with halos of dark matter particles picked out using a standard friends-of-friends algorithm which collects particles in groups which have neighbours with separations r_{ll} smaller than ll (*linking length*) times the mean inter particle spacing $\Delta x = \bar{r}^{1/3}$

$$r_{ll} \leq ll \cdot \Delta x. \quad (1)$$

This group finding algorithm does not assume a special geometry for the identified objects, but it is based only on particle positions. It picks out particle groups for which the density in the outer parts corresponds to the value found from the theory of a spherical top hat collapse.

Table 2. Linking lengths ll for the different models used with the friends-of-friends algorithm and the percentage of identified unvirialized particle groups. The mass cut is measured in $10^{14} h^{-1}\text{M}_\odot$ which corresponds to 25 particles.

	ll	δ_{TH}	unvirialized halos	mass cut
SCDM	0.20	178	7 %	0.28
ΛCDM	0.16	334	4 %	0.22
OCDM1	0.15	402	1 %	0.22
OCDM2	0.17	278	3 %	0.38

The density contrast $\delta_{\text{TH}} = (\rho - \bar{\rho})/\bar{\rho}$ for a spherically symmetric (top-hat) collapse in an Einstein-de-Sitter universe is $\delta_{\text{TH}} \approx 178$. For an isothermal density profile $\rho(r) \propto 1/r^2$ this value corresponds to the linking length $ll = 0.2$ (Lacey & Cole 1994). The linking length for gravitationally bound objects in open and Λ -universes is given by

$$ll(\delta_{\text{TH}}) = 0.2 \left(\frac{178}{\delta_{\text{TH}}(\Omega_0, \Omega_{\Lambda,0})} \right)^{1/3}. \quad (2)$$

The values of ll listed in Table 2 are based on eq. 2 where the values of $\delta_{\text{TH}}(\Omega_0, \Omega_{\Lambda,0})$ are calculated from the formula found in Katayama & Suto (1996).

However, it is not clear whether the FOF groups really lead to gravitationally bound and virialized groups. The algorithm might link two (or more) smaller groups connected by a tenuous bridge of particles. The group members could also be random encounters, particles or particle groups that fly by at the

moment of identification, or what we will see later, are ongoing merging events. To check for such effects we explicitly tested the virial theorem $|E_{\text{pot}}| = 2 E_{\text{kin}}$ for each individual halo. This seems to be a reasonable procedure since virialisation is a very fast process in nature, and since unvirialized objects may be identified with particular processes within the hierarchical structure formation scenario.

Following Spitzer (1969), the potential energy can be approximated by

$$|E_{\text{pot,approx}}| \approx 0.4 G \frac{M^2}{r_h}, \quad (3)$$

where r_h is the half-mass radius of the system. For the smaller halos the potential energy calculated using eq. 3 can be compared with the direct summation

$$|E_{\text{pot,direct}}| = \sum_{i=1}^N \sum_{j=i+1}^N G \frac{m_i m_j}{|r_i - r_j|} \quad (4)$$

This shows that the factor 0.4 is a good choice for most of the clusters.

$$|E_{\text{pot,approx}}| \lesssim |E_{\text{pot,direct}}| \quad (5)$$

Therefore, the approximation given by eq. 3 is used throughout the further analysis.

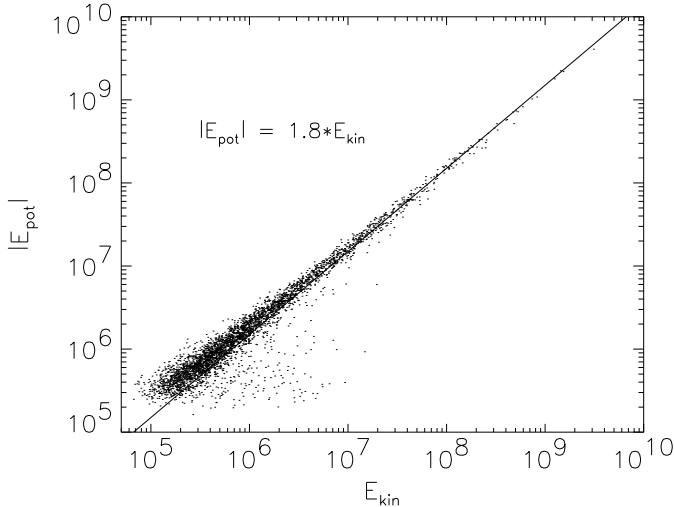


Fig. 2. Virial theorem for clusters in the Λ CDM model (units are arbitrary).

The kinetic energy of an identified object is calculated by summing over all particle velocities with respect to the motion of the cluster centre

$$E_{\text{kin}} = \frac{1}{2} \sum_{i=1}^N m_i (\mathbf{v}_i - \mathbf{v}_{\text{centre}})^2. \quad (6)$$

Since all particles have the same mass $m \equiv m_i$ the kinetic energy can be connected to the velocity dispersion,

$$\sigma_v^2 = \frac{2}{Nm} E_{\text{kin}}. \quad (7)$$

Fig. 2 shows the virial relation as a scatter plot for all particle groups identified in the Λ CDM model at a redshift of $z = 0$. The ‘lower’ virial relation shown by the straight line, $|E_{\text{pot}}| \approx 1.8 E_{\text{kin}}$, can be understood as the influence of an outer pressure of radially infalling particles into the halos (Cole & Lacey 1996). The bend of the virial relation at low energies towards the theoretical expectation proves that the surface influence becomes less important for groups of small particle numbers, i.e. their stage is less influenced by a steady accretion rate than the high mass halos. An opposite effect concerns a much smaller number of groups with velocity dispersions which are too high compared to their potential energy. These clusters are considered unvirialized and are treated separately in the following analysis, and are investigated in detail. There are many more unvirialized FOF-groups of low and intermediate richness. In Table 2 we give the percentage of unvirialized objects among all FOF clusters for the different cosmological models. It becomes obvious that the percentage of unvirialized groups is highest in SCDM and lowest in OCDM1. This reflects to early formation of groups in low Ω_0 models, but also the Λ CDM model has a higher percentage of unvirialized groups in comparison to OCDM1.

Now we investigate in more detail the nature of the halos that are not gravitationally bound.

3.1. Velocity Dispersion – Mass

First we discuss the correlation of velocity dispersion and the mass of virialized and unbound groups. We expect a tight correlation of both quantities for virialized objects if we assume an isothermal sphere for the halo and a cutoff at constant density, which can easily be taken to be the mean cosmic density of the halos at the time when they form or suffer their last big merger. Since most halos form quite recently this cutoff is almost constant, and we get

$$\sigma_v = V_c / \sqrt{2} \propto M^{1/3}. \quad (8)$$

As can be seen from Fig. 3 this is represented very well in our simulations with a large scatter for the light clusters which was also found by Cole & Lacey (1996); we have fitted the data for the virialized particle groups to the scaling relation $\sigma_v \propto M^\alpha$ where α was found to be exactly 1/3. Fig. 3 also suggests that the unvirialized objects mostly lie at the low mass end of the distribution with high velocity dispersions. Cole & Lacey (1996) argue that the tail of groups with $\sigma_v > V_c / \sqrt{2}$ likely represent objects that belong to larger virialized structures. But if we repeat our analysis using a larger linking length ll we derive similar results: even for FOF groups identified with a linking length corresponding to an over-density $\delta \ll \delta_{\text{TH}}$ we find unbound groups in the tail $\sigma_v > V_c / \sqrt{2}$ in contradiction to the claim of Cole & Lacey (1996). It should be mentioned that at the low mass end the FOF groups are not well resolved because these objects consist only of few particles. More interesting than the low mass groups are the small number of halos of all masses, lying beneath the virial relation

$\sigma_v = V_c/\sqrt{2}$. They represent groups in the process of merging which are unbound because they are too extended. In most cases they represent halos with more than one centre which are connected by slight tidal bridges and similar structures. These systems are not very frequent, i.e. they do not survive for a long time, but they mark most interesting places in the simulation box. And it can be expected that they are sites for active structure formation processes in nature.

The results for the different cosmological models introduced in Table 1 are comparable and therefore we only a plot for the Λ CDM model is presented.

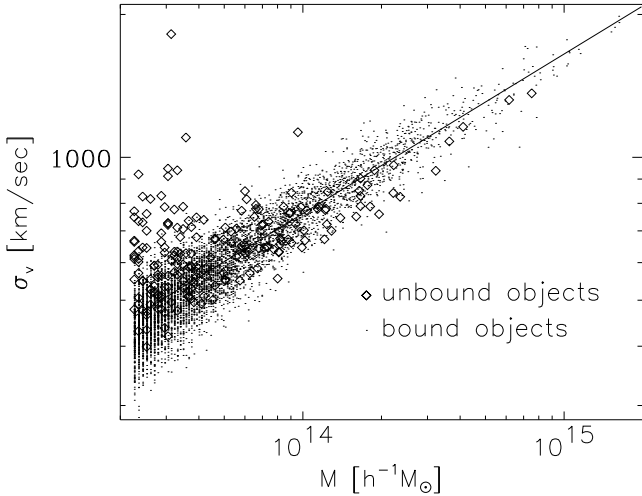


Fig. 3. Relation between velocity dispersion and the mass for the Λ CDM model. The virialized halos are marked with points and the objects that are not in virial equilibrium are marked using diamonds. The solid line is a fit to the scaling relation $\sigma_v \propto M^{1/3}$.

3.2. Eigenvalues of the Inertia Tensor

The next point we are going to investigate is the shape and the axis ratios of the identified galaxy clusters. To this aim we calculate the eigenvalues of the inertia tensor for each FOF group, which are given in the order $a > b > c$. In Fig. 4 we show a scatter plot of the ratios of the eigenvalues for the Λ CDM-simulation at $z = 0$. In this plot, spherical groups are situated in the upper right corner, oblate clusters in the right and prolate clusters in the upper part. It is well known (Dubinsky 1992, Warren et al. 1992, Cole & Lacey 1996) that hierarchical clustering leads to triaxial ellipsoids with a typical axis ratio of 1:0.7:0.5 which is well represented by our simulations.

The unvirialized halos inhabit more the lower left part of the diagram, again characterizing the soft merging, i.e. the elongation of the groups due to tidal interaction of the progenitors which marks the direction of the encounters, and in some cases to an elongation of the clusters in a second direction due to non-central encounters. Typically unvirialized clusters have an axis ratio of 1:0.4:0.3, i.e. they are more oblate and in general deviate stronger from sphericity than virialized clusters.

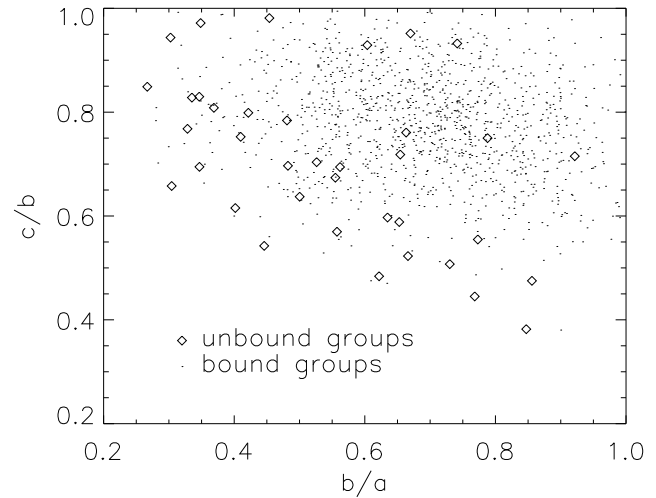


Fig. 4. Axis ratio of virialized (dots) and unvirialized groups (diamonds) for the Λ CDM-simulation at $z = 0$.

These findings again to not depend strongly on the the cosmological background model. We get similar axis ratios when looking at the SCDM or the OCDM2 model.

3.3. Impact Parameters

Let us now discuss how the impact parameter and the relative motion between mergers influences the virialisation of the merger products. To this aim we consider merging events occurring from redshift $z = 0.1$ to $z = 0.0$ between particle groups containing more than 25 particles, and we specialize on halos for which the mass ratio of the two most massive progenitors is greater than 1/3. The results are listed in Table 3 where we have neglected the analysis of the OCDM1 model; this model is outstanding because of our normalisation. It does not produce enough galaxy clusters so that the examination of merging events will not provide reasonable results as can be seen by the very low percentage of unvirialized objects in Table 2.

Table 3. Mean values for the impact parameter (in h^{-1} Mpc) separated for virialized and unvirialized objects.

	virialized objects	unvirialized objects
SCDM	0.92 ± 0.60	1.19 ± 0.59
ΛCDM	0.91 ± 0.45	1.18 ± 0.48
OCDM2	0.91 ± 0.48	1.26 ± 0.50

Using the same constraints on the identification of mergers we have calculated the mean values for the impact velocities. The results can be found in Table 4 and show that the two most massive progenitors of clusters that are identified to be not in virial equilibrium collide with slightly higher velocities compared to the impact velocities of progenitors leading to virialized objects.

Table 4. Mean values for the impact velocities (in km/s) separated for virialized and unvirialized objects.

	virialized objects	unvirialized objects
SCDM	670 ± 500	900 ± 450
ΛCDM	560 ± 300	600 ± 280
OCDM2	640 ± 380	830 ± 350

As we can see from Table 3 the mean value of the impact parameter for non-virialized particle groups is slightly larger than the corresponding value for bound objects. This again is a hint for a merging event where the two progenitors had not enough time to relax to a gravitational bound object, they have just started to conflate.

3.4. Virialisation

If the unvirialized objects are ongoing mergers they should lead to gravitational bound objects after a short phase of relaxation. This is going to be checked now. We identify unvirialized particle groups at a redshift of $z = 0.1$ (0.2) and have a look at the percentage of these objects that are found to be in virial equilibrium at a redshift of $z = 0.0$ (0.1).

Table 5. Percentage of objects that have virialized from redshift $z = 0.2$ to $z = 0.1$ and $z = 0.1$ to $z = 0.0$. Again a masscut of 25 particles has been used.

	$z = 0.2 \rightarrow z = 0.1$	$z = 0.1 \rightarrow z = 0.0$
SCDM	$(74 \pm 4) \%$	$(63 \pm 4) \%$
ΛCDM	$(46 \pm 6) \%$	$(90 \pm 5) \%$
OCDM2	$(83 \pm 7) \%$	$(84 \pm 7) \%$

We can see that most of the unbound particle groups virialize between the considered redshifts, for the Λ CDM model nearly all objects have settled to virial equilibrium within the redshift interval $z = 0.1 \rightarrow z = 0.0$. This shows that the time during which the cluster is unbound is very short, virialisation is a fast process. The low percentage for the Λ CDM model at the early redshift can be explained, because we have found that most of the halos had heavy interaction with the surroundings from redshift $z = 0.2$ to $z = 0.1$, and so they remained in their non virial state. Additionally some of the objects identified at redshift $z = 0.2$ do not exist anymore at the later redshift: they got disrupted by tidal forces from nearby objects.

Fig. 5 shows the most massive unvirialized cluster in the SCDM simulation at $z = 0$ ($M = 3 \cdot 10^{13} h^{-1} M_{\odot}$) and its two almost equal mass progenitors at $z = 0.1$. Obviously this is quite a soft merger which means that the relative velocity at $z = 0.1$ is not much larger than the inner velocity dispersion. The progenitors perform an almost central encounter, during which only a small orbital angular momentum is transferred to increase the spin of the resulting halo, and there is a quick settling into a new virial equilibrium as the small percentage of

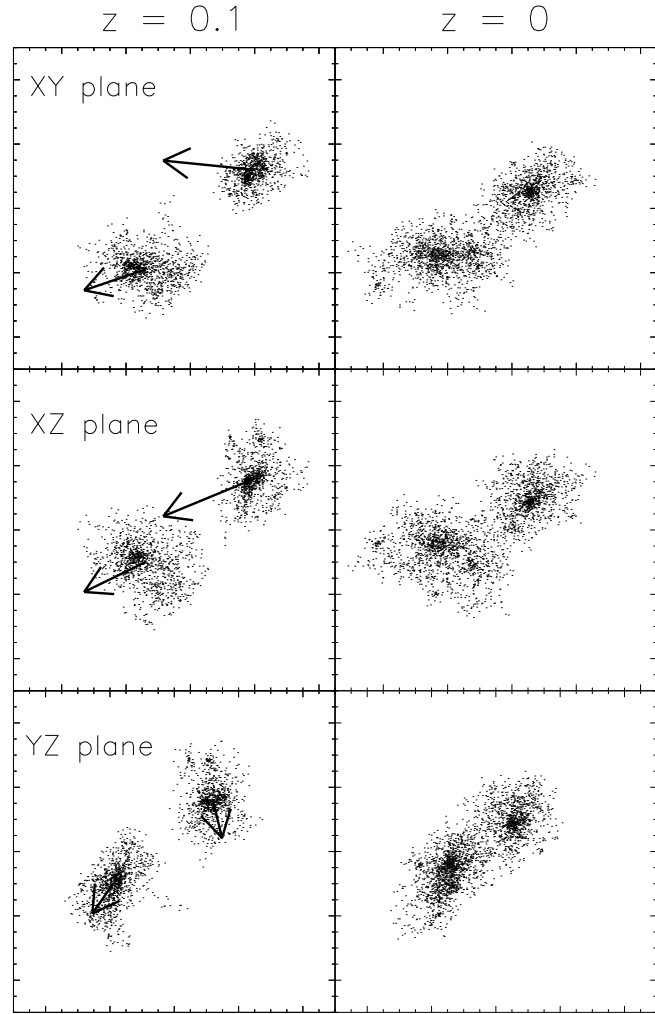


Fig. 5. Projections of a cube of $(10h^{-1} \text{Mpc})^3$ of the SCDM simulation box at redshifts $z = 0.1$ and $z = 0$, containing the most massive unvirialized cluster. Only the particles in the cluster and in the two most massive progenitors are shown which are both virialized objects.

unvirialized objects proves. The absolute value of the velocity vector shown in this plot is arbitrary, just the direction and the relative lengths are correct to give an impression of how the two progenitors collide.

4. Correlation functions

One of the basic constraints of cosmological models is the shape and the amplitude of the two-point correlation function. For many years it has been the standard way to describe the clustering of galaxies and galaxy clusters. The assumption that galaxies (and clusters) only form from high-density regions above some threshold value δ_c leads to a correlation of points exceeding this value δ_c that is enhanced in comparison to the dark matter correlation function (Kaiser 1984). This effect suggests the introduction of a biasing parameter b ,

$$\xi_{\text{cluster}}(r) = b^2 \xi_{\text{mass}}(r). \quad (9)$$

But it is by no means compelling that the bias factor is independent of scale as we can see from Table 6 and Fig. 6.

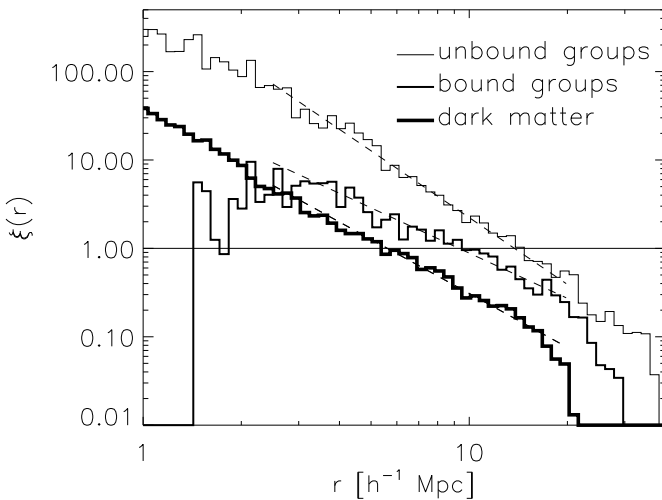


Fig. 6. Correlation functions for the Λ CDM model. Histograms from below (at $r > 3h^{-1}\text{Mpc}$) denote dark matter particles, virialized clusters (fixed number density of $n = 10^{-5}h^3\text{Mpc}^{-3}$) and unvirialized groups. The dashed lines are fits with parameters specified in Table 6.

If we apply this correlation statistics to our simulations we find that the unvirialized objects are more strongly correlated than the relaxed systems. In Fig. 6 we show this result again only for the Λ CDM model. We find that the correlation between virialized groups lies only a factor two over the correlation function of dark matter. We fitted standard power laws

$$\xi(r) = (r_0/r)^\gamma \quad (10)$$

which are shown in the Fig. 6 as dashed lines. Galaxy groups in the Λ CDM model have a correlation length $r_0 \sim 9 h^{-1}\text{Mpc}$ and a slope $\gamma = 1.7$. The correlation function turns negative beyond $30 h^{-1}\text{Mpc}$. Fits for the other models are given in Table 6. To get comparable values for the different cosmologies we fixed the cluster number density to $n = 10^{-5}h^3\text{Mpc}^{-3}$ and used only the $N = nV$ most massive clusters for the calculation of the correlation function (values for N are given in Table 6, too). Obviously the amplitude in SCDM and OCDM2 are smaller than in the Λ CDM model, i.e., these models have too small power on large scales for describing the clustering of groups and clusters of galaxies.

In Table 7 we demonstrate the strong dependence of the amplitude of the correlation function on the mass cuts. High mass halos mark high density maxima in the dark matter distribution which are stronger clustered (Kaiser 1984). The slope remains almost unchanged. Due to the smallness of the simulation box it is difficult to compare with the correlation function of rich clusters of galaxies which are identified with halos of mass larger than $2 \cdot 10^{14} h^{-1}\text{M}_\odot$. It is interesting that the bound halos in the SCDM model have the lowest amplitude among all models. This is connected with the high evolution

Table 6. Fit parameter of the correlation functions for dark matter (first column), bound clusters (second column) and unbound clusters (third column) for three cosmological models.

	dark matter		bound groups			unbound groups	
	r_0	γ	r_0	γ	N	r_0	γ
SCDM	5.4	2.3	6.6	1.8	800	9.2	2.5
ΛCDM	5.6	2.0	9.3	1.7	2200	13.8	2.5
OCDM2	4.5	2.2	7.9	2.0	2200	11.4	2.5

Table 7. Parameter for the correlation functions calculated for different mass cuts for the virialized halos. The mass cut is given as the number of particles.

mass cut	SCDM		ΛCDM		OCDM2	
	r_0	γ	r_0	γ	r_0	γ
25	4.0	2.1	6.2	1.8	5.6	1.7
50	4.5	1.8	8.3	1.7	6.7	1.9
100	5.1	1.7	9.1	1.7	8.4	2.1

stage of this model where very big halos form which include most of the matter in the simulation box, and on the other hand with the small power of SCDM at large with respect to small scales, this being related to the high value of $\Gamma = 0.5$. Observations lead to a preferred value of $\Gamma = 0.25 \pm 0.05$ (Peacock & Dodds 1996).

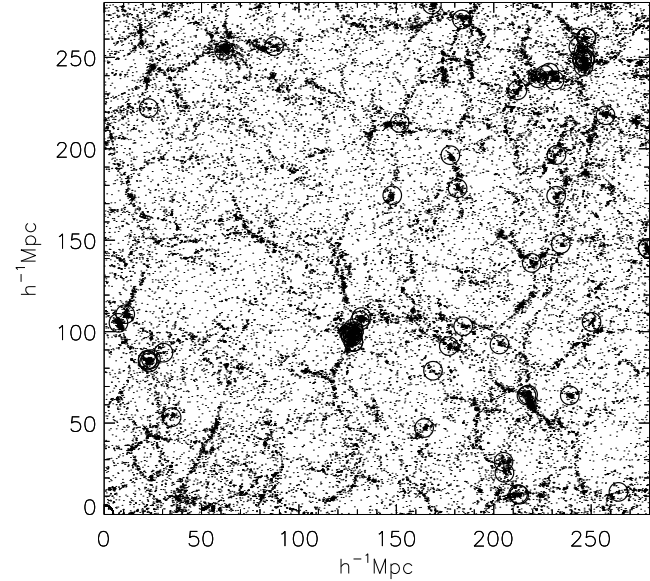


Fig. 7. Slice through the Λ CDM simulation. The circles indicate the positions where unvirialized objects have been found.

But most interesting is the correlation function of the unvirialized particle groups. They are much more strongly clustered than virialized objects, and the slope is very steep, $\gamma = 2.5$, independent of the cosmological model, cf. Table 6. This verifies that mergers are occurring at particular places in the

universe, and that these processes are highly correlated. This can be checked in Fig. 7. We have plotted a slice through the Λ CDM simulation and marked the places where unvirialized objects have been identified with circles. These objects are found preferably in high density regions whereas virialized halos trace the overall large scale structure of the universe.

Nowadays it seems clear that strong interactions and mergers are the trigger for producing the most luminous infrared galaxies. So an enhanced clustering has been obtained for luminous infrared galaxies (Bouchet et al. 1993). More luminous IRAS galaxies, basically mergers, are more strongly correlated, and ultraluminous mergers have strongest correlation strength (Gao 1993). These luminous infrared galaxies may represent an important stage in the formation of QSO's and a primary stage in the formation of elliptical galaxies cores. And as we have found, these objects form at special places in the universe where the most massive galaxy clusters are found.

5. Conclusions

We have collected a number of reasons for looking at virialisation as a reasonable criterion for identifying groups and clusters of galaxies in numerical simulations. The virial theorem well described an overwhelming majority of the halos in our simulations. A slight bend in the virial relation can be ascribed to the effective pressure of the permanent spherical accretion stream in the halos.

Special attention has been devoted to the unvirialized halos. We have shown that they are characterized by quite recent soft mergers which lead to more anisotropic halos and are strongly correlated over scales of up to $40 h^{-1}$ Mpc. This is confirmed by the result obtained for luminous infrared galaxies. In our simulations we find a very fast virialisation of the halos which leads to the small percentage of such objects at any given time. But the virialisation itself was not a basic goal of our simulations. It must be checked whether this time depends on the relatively low mass resolution in our big simulation boxes. The SCDM model is found to have the largest evolution rate of the halo abundance to $z = 0$, and has the largest percentage of unvirialized objects. On the contrary, the more realistic Λ CDM and OCDM2 models have a quite small number of recent mergers.

The stronger anisotropy of the merger products leads to typical triaxial ellipsoids with axis ratios of 1:0.4:0.3 which represents an measurable effect in large cluster samples. The merging processes are characterized by basically central encounters. Not much angular momentum is transferred to the merger product which leads to a self-similar growth of the rotation of the halos, (e.g. Knebe 1998).

The large differences in the correlation functions of the models makes it worthwhile to further compare differences in the large-scale matter distributions of the different models.

Acknowledgements. We are grateful to H. Couchman for making his numerical code public. Also we acknowledge the use of CMBFAST provided by U. Seljak and M. Zaldarriaga. We are glad about use-

ful and encouraging discussions with J. Colberg, S. Gottlöber and D. Woods read carefully the manuscript and made valuable comments.

References

Bouchet F.R., Strauss M.A., Davis M., Fisher K.B., Yahil A., Huchra J.P., *ApJ* **417**, 36 (1993)
 Bunn E.F., White M., *ApJ* **480**, 6 (1997)
 Cole S., Lacey C., *MNRAS* **281**, 716 (1996)
 Couchman H.M.P., *ApJ* **368**, L23 (1991)
 Couchman H.M.P., Thomas P.A., Pearce F.R., *ApJ* **352**, 797 (1995)
 Davis M., Efstathiou G., Frenk C. S., White S.D.M., *ApJ* **292**, 371 (1985)
 Dubinski J., *ApJ* **401**, 441 (1992)
 Einasto J., Einasto M., Tago E., Starobinsky A.A., Atrio-Baradela F., Müller V., Knebe A., Frisch P., Cen R., Andernach H., *ApJ* submitted (1997)
 Gao, Y., in: *The Evolution of Galaxies and Their Environment*, eds. Hollenbach, D., Thronson, H., Shull, J.M., NASA Conf. Pub. 3190, Ames: NASA 1993, 54
 Gelb J., Bertschinger E., *ApJ* **436**, 467 (1994)
 Jing, Y.P., Mo, H.J., Börner, G., Fang, L.Z., *MNRAS* **276**, 417 (1995)
 Kaiser N., *ApJ Lett.* **284**, L9 (1984)
 Katayama T., Suto Y., *ApJ* **469**, 480 (1996)
 Knebe A., in: *Large Scale Structures: Tracks and Traces. Proceedings of the 12th Potsdam Cosmology Workshop*, ed. V. Müller et al. , World Scientific 1998, p. 175
 Klypin A., Gottlöber S., Kravtsov A.V., (astro-ph/9708191)
 Lacey C., Cole S., *MNRAS* **262**, 627 (1993)
 Lacey C., Cole S., *MNRAS* **271**, 676 (1994)
 Mohr J.J., Evrard, A.E., Farcanci, D. G., Geller, M.J., *ApJ* **447**, 8 (1995)
 Peacock J. A., Dodds S.J., *MNRAS* **280**, 1020 (1996)
 Seljak U., Zaldarriaga M., *ApJ* **469**, 437 (1996)
 Spitzer L., *ApJL* **158**, 139 (1969)
 Thomas P.A., Colberg J.M., Couchman H.M.P., Efstathiou G.P., Frenk C.S., Jenkins A.R., Nelson A.H., Hutchings R.M., Peacock J.A., Pearce F.R., White S.D.M. *MNRAS* submitted (astro-ph/9707018)
 Warren M.S., Quinn P.J., Salmon J.K., Zurek W.H., *ApJ* **399**, 405 (1992)
 White S.D.M., in: *Cosmology and Large-Scale Structure*, eds. Schaeffer R., Silk J., Spiro M., Zinn-Justin J., Elsevier 1996, p. 349